



Article

Analysis of Phase Transformations in Fe-Ni-Al Alloys Using Diffusion Couples of Fe/Fe-33at.%Ni-33at.%Al Alloy/Ni

Eduardo Perez-Badillo, Hector J. Dorantes-Rosales, Maribel L. Saucedo-Muñoz  and Victor M. Lopez-Hirata * 

Department of Metallurgy and Materials, ESIQIE, Instituto Politécnico Nacional, Mexico City 07300, Mexico; eperezb1105@alumno.ipn.mx (E.P.-B.); hdorantes@ipn.mx (H.J.D.-R.); msaucedom@ipn.mx (M.L.S.-M.)

* Correspondence: vmlopezh@ipn.mx; Tel.: +52-5557-296-000 (ext. 54205)

Abstract: The present work focused on analyzing the phase transformation in Fe-Ni-Al alloys employing a diffusion couple of Ni/Fe-Ni-Al/Fe, and Calphad-based diffusion and thermodynamic software. Diffusion couples were prepared by annealing at 1100 °C for 200 h and then air-cooled. These couples were also aged at 750 °C for 100 and 275 h. Both numerical and experimental results indicated that the diffusion path between Ni or Fe pure metal and the Fe-33at.%Ni-33at.%Al alloy is not linear. The phases formed during the diffusion anneal at 1100 °C correspond to those shown in the Calphad-calculated Fe-Ni-Al equilibrium diagram. The aging treatment at 750 °C promoted the inverse precipitation $\beta' \rightarrow \beta' + \alpha$, which caused the softening of the alloy. Moreover, the normal precipitation reactions, $\alpha \rightarrow \alpha + \beta'$ and $\gamma \rightarrow \gamma + \gamma'$, were also observed to occur during the aging of diffusion couple at 750 °C, originating precipitation hardening.

Keywords: Fe-Ni-Al alloys; diffusion-couples; β' precipitates; γ' precipitates; aging; precipitation hardening



Citation: Perez-Badillo, E.; Dorantes-Rosales, H.J.; Saucedo-Muñoz, M.L.; Lopez-Hirata, V.M. Analysis of Phase Transformations in Fe-Ni-Al Alloys Using Diffusion Couples of Fe/Fe-33at.%Ni-33at.%Al Alloy/Ni. *Metals* **2023**, *13*, 1221. <https://doi.org/10.3390/met13071221>

Academic Editor: Angelo Fernando Padilha

Received: 31 May 2023

Revised: 28 June 2023

Accepted: 29 June 2023

Published: 1 July 2023



Copyright: © 2023 by the authors. Licensee MDPI, Basel, Switzerland. This article is an open access article distributed under the terms and conditions of the Creative Commons Attribution (CC BY) license (<https://creativecommons.org/licenses/by/4.0/>).

1. Introduction

The mechanical strength at high temperatures for Ni-based superalloys depends strongly on the presence of fine coherent particles of γ' (Ni_3Al) with an ordered crystalline structure $\text{L}1_2$ in the γ phase matrix. Nevertheless, prolonged service at high temperatures and the cyclic heating of turbines may promote the coarsening of γ' precipitates, which originates the loss of its coherency between precipitates and matrix. These microstructure changes may affect the mechanical performance of components because of the deterioration of their mechanical strength [1–6]. Ferritic alloys strengthened with coherent precipitates show great potential for key applications in aerospace, power industries, shipbuilding, and automotive components due to their excellent mechanical properties and low cost [7,8]. In recent years, the development of new intermetallic compounds has become an essential point for application to the precipitation hardening of alloys at high temperatures [9]. For instance, the phase transformations of Fe-Ni-Al alloys are important for developing different industrial alloys, such as superalloys, stainless steels, ferritic steels, maraging steels, and light steels [9–16]. The precipitated phases, such as the β' phase with a NiAl-type crystalline structure, are important for this purpose, and they may originate the precipitation hardening of the ferritic matrix [17–24]. This precipitation is expected to harden the Fe-Ni-Al alloys similarly to that of the γ' precipitates since the interface between the precipitate and matrix is coherent, which may help to generate good coarsening resistance. The content of alloying element plays a crucial role in the precipitation reaction, growth kinetics, and mechanical properties of the alloys [25–30]. For example, Contreras-Piedras et al. [31] pointed out that the hardness of Fe-Ni-Al alloys increased with increasing the content of Al and Ni (>15 at.%) because of a higher volume fraction of β' precipitates. However, the coarsening resistance of precipitates also decreased, which may cause a decrease in hardness. The effect of different alloying is a research topic of interest. For instance, Dong et al. [32] showed

that the V addition strongly affected the formation of the γ phase during air-cooling in Fe-Mn-Al-Ni alloys. In the same way, Park et al. [33] observed that the mean radius of the NiAl precipitates gradually decreased with an increase in vanadium concentration. This produced an enhanced yield strength from 210 MPa to 401 MPa at 973 K in compressive tests in Fe-Cr-Ni-Al-V system. Furthermore, the coarsening growth kinetics of precipitates also relates to the alloying content. For example, Eris et al. [34] analyzed the Hf, Hf-Mo, and Hf-W additions to Ni-based superalloys. They also stated that the coarsening rate of γ' -Ni₃Al-X precipitates decreases with the increase in addition of Hf-Mo and Hf-W. In contrast, the addition of only Hf originates a faster coarsening rate of γ' precipitates, which may promote their dissolution at the early stages. This content may change the coherency between the matrix and the precipitate, the solubility in the matrix phase, and the atomic diffusivity. To exhibit high coarsening resistance in precipitates during the heating of alloys, a low interfacial free energy between the matrix and precipitate, low solubility, and a slow diffusion process are essential characteristics to keep the mechanical properties at high temperatures during the service operation of the industrial components [25–29]. Baik et al. [35] noted that the increase in Ti gradually increased their mechanical strength from 1237 to 1538 MPa for a content of 3.5 wt.% Ti. This behavior is due to the increase in the volume fraction of precipitates L2₁ formed inside the β' phase. These precipitates improve the lattice misfit, increasing the coherency between the precipitate and matrix. However, the mechanical strength decreases to 1402 MPa for a content of 4 wt.% Ti because of the transformation of the β' phase into the L2₁ phase.

The use of diffusion couples [36–38] has been a powerful traditional tool to determine binary- and ternary-phase diagrams. The diffusion couple method has also permitted following the growth kinetics of phases formed in the alloy system. Thus, this method is a good alternative to analyze the phase formation in different Fe-Ni-Al alloy compositions. This method permits obtaining the equilibrium phases for a phase diagram. Additionally, the aging of the diffusion couple enables us to analyze the precipitation process for different alloy compositions using the same specimen.

Nowadays, the application of Calphad-based software such as Thermo-Calc and DICTRA (Thermo-Calc Software, Stockholm, Sweden) [39–41] enables to analyze the equilibrium phases either in a phase diagram or in a diffusion couple using numerical solutions of the diffusion equations for multicomponent alloys. The DICTRA software employs atomic mobility, which permits considering the thermodynamic interaction among alloying elements during atomic diffusion. This fact suggests that the annealing of a diffusion couple can be simulated even for ternary alloy systems. Additionally, the Thermo-Calc software also permits following the phase formation in equilibrium at different temperatures for these alloys. This software also permits studying the possible precipitation process after aging treatment, as well as the chemical and structural characteristics of the matrix and precipitate phases.

Therefore, this work aims to study the phase formation and precipitation process of Fe-Ni-Al alloys using diffusion couples and Calphad-based computer programs to understand their corresponding properties at high temperatures.

2. Materials and Methods

2.1. Numerical Method

The temporal evolution of concentration profiles for a diffusion couple can be expressed by Fick's second law [40]:

$$\frac{\partial c_k}{\partial t} = -\nabla(j_k) \quad (1)$$

where c_k is the concentration of the k element, and the diffusion flux j_k for a multicomponent system is given by the Onsager equation [40]:

$$j_k = -\sum_{j=1}^n D_{kj}^n \frac{\partial c_j}{\partial z}. \quad (2)$$

where D_{kj}^n is the chemical diffusion coefficient for each of the n components, and they can be expressed as [40]:

$$D_{kj}^n = -\sum_{j=1}^n L'_{kj} \frac{\partial \mu_i}{\partial c_j}. \quad (3)$$

where μ_i is the chemical potential for the different elements, and L_{kj} is a proportionality factor, which depends on the element mobility, and it is given by:

$$L_{kj} = (\delta_{ik} - c_k V_i) \cdot c_i M_i \quad (4)$$

where δ_{ik} is the Kronecker delta, and V_i and M_i are the partial molar volume and mobility of component i , respectively. The mobility M_i is defined as follows:

$$M_i = \frac{M_i^0}{RT} \exp\left(-\frac{Q_i}{RT}\right). \quad (5)$$

where M_i^0 is a frequency factor and Q_i is the activation energy, which depend on the chemical composition and the temperature.

The diffusion process of the diffusion couple was numerically simulated using Thermo-Calc DICTRA [42] and the TCFE11 and MOFE6 databases (Thermo-Calc Software, Stockholm, Sweden). The modeling of the diffusion couple was carried out in the fcc austenite phase using a planar morphology. Moreover, the ternary Fe-Ni-Al phase diagrams at different temperatures were calculated with Thermo-Calc (TC) [43]. It is important to mention that the diffusion coefficients D and mobilities M were taken from references [44–47].

Moreover, the precipitation process for Fe-Ni-Al alloys was carried out using the TC-Prisma software (Thermo-Calc Software, Stockholm, Sweden) and also using TCFE11 and MOFE6 databases (Thermo-Calc, Stockholm, Sweden). The thermodynamic and diffusion data were taken, for example, from references [48–50]. The precipitation simulation considered the bulk nucleation of either the α or β' phases in the β' and α matrix phase during the isothermal aging. The interfacial free energy between the precipitate and matrix was also calculated by TC-Prisma. The energy values correspond to a coherent interface, as expected for this type of precipitation [12,17,51]. TC-Prisma enables us to analyze the precipitation process in a concomitant way of the nucleation, growth, and coarsening of precipitates.

2.2. Experimental Method

An Fe-33at.%Ni-33at.%Al alloy was fabricated with high-purity pure Fe, Ni, and Al metals (>99.9%) using an Edmund Bühler Compact Arc Melter (Edmund Bühler GmbH, Schindäckerstraße, Bodelshausen, Germany). A tungsten electrode and Ar gas atmosphere were used during the melting process. Alloy, pure Fe, and Ni plate specimens of $5 \times 10 \times 4$ mm were obtained by machining. For the metallography preparation of the most prominent face, we used up to 2000 grit number emery paper, alumina of 0.5 μm , and silica colloidal of 0.02 μm . The diffusion couple of Fe/Fe-33at.%Ni-33at.%Al alloy/Ni was kept together using an austenitic stainless-steel specimen holder. This specimen holder was encapsulated in a quartz tube under an Ar gas atmosphere. The diffusion annealing was carried out at 1100 °C for 72 h using an electric furnace. The diffusion couple was sectioned into specimens of 3 mm length to conduct aging treatments using a Struers Minitom (Struers S.A.S, Champigny sur Marne, France) cutting apparatus. These specimens were quartz-encapsulated with Ar gas, and then solution-treated at 1100 °C for 1 h, air-cooled, and subsequently aged at 750 °C for 100 and 250 h using a Carbolite electric

furnace (Carbolite Gero GmbH & Co. KG, Neuhausen, Germany). The aged specimens were metallographically prepared, as explained above, and then electrochemically etched with an electrolyte of 10 vol.% HCl in CH₃-OH at 3 V dc for 3–4 s. All specimens were observed with an EDX-equipped scanning electron microscope, JEOL JSM-6701F SEM (JEOL USA Inc., Dearborn Road Peabody, MA, USA), at 20 kV using secondary electrons. The Vickers microhardness was pursued on the aged specimens with a load of 100 g and a dwell time of 12 s. Microhardness indentations were pursued for positions with an interval of about 100 microns on the same line, considering the Fe/Fe-NiAl alloy and Ni/Fe-Ni-Al alloy interfaces as the origin, and for four lines separated from each other by approximately 500 microns. An average hardness was determined for four values.

3. Results and Discussion

3.1. Phase Stability and TTT Diagram

Figure 1 shows the experimental and TC-calculated Fe, Ni, and Al concentration profiles corresponding to the diffusion couple sides Fe/Fe-Ni-Al alloy/Ni and Ni/Fe-Ni-Al alloy after diffusion annealing at 1100 °C for 72 h. The experimental values in the colored symbols show, in general, good agreement with the calculated colored lines. This result indicates that the diffusion of Fe into the Fe-Ni-Al alloy with an fcc structure is slower than that of Ni with an fcc structure. This fact is attributable to the fastest atomic interdiffusion of Ni-rich Ni-Fe alloys because of their lower activation energy Q , 312 kJ mol⁻¹ compared to 318 kJ mol⁻¹ for Fe-rich Fe-Ni alloys [52]. Likewise, Al from Fe-Ni-Al alloy diffused faster into the Ni side than into the Fe side, which is attributable to the lower activation energy Q , 272 kJ mol⁻¹ compared to 339 kJ mol⁻¹ for Fe-rich Al-Ni alloys [42].

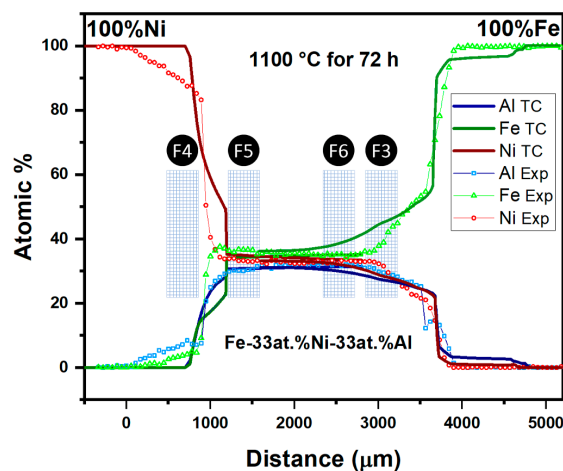


Figure 1. Experimental and TC-DICTRA-calculated concentration profiles of Fe, Ni, and Al for the Fe/Fe-Ni-Al/Ni diffusion couple after diffusion annealing.

The Thermo-Calc-calculated Fe-Ni-Al ternary-phase diagrams are shown in Figure 2a,b at 750 and 1100 °C, respectively. These figures also show the experimental values of chemical composition determined in the diffusion couples, as indicated by the red triangle marks. Figure 2b suggests that the diffusion path between the diffusion couples of Fe/FeNiAl alloy and Ni/FeNiAl alloy is not linear but sinusoidal, as expected for ternary alloy systems [52–54]. The following phase sequence presents the diffusion path for the Fe/FeNiAl alloy diffusion couple at 1100 °C:



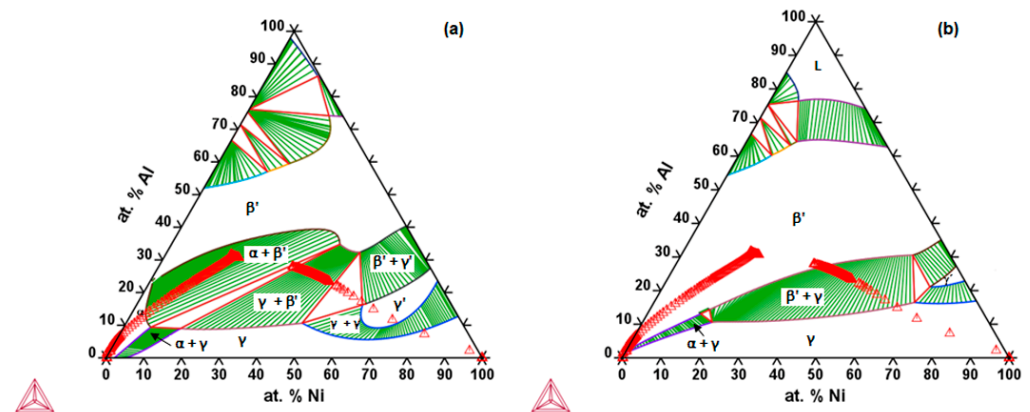


Figure 2. TC-calculated Fe-Ni-Al phase diagram at (a) 750 °C and (b) 1100 °C.

Fe γ is the fcc austenite, α the bcc ferrite phase, β' the NiAl-type intermetallic compound, and γ' the Ni-rich fcc phase. The β' phase is responsible for increasing the mechanical strength during the precipitation hardening of Fe-based superalloys [10,12,14,17,31]. The β' precipitate phase is coherent with the α ferrite phase. This fact causes a more effective increase in mechanical strength, as well as an increase in coarsening resistance, which permits keeping their mechanical strength at high temperatures.

On the other hand, the phase diffusion path of the Ni/FeNiAl alloy diffusion couple at 1100 °C is as follows:



Table 1 presents the Thermo-Calc (TC)-calculated chemical compositions of the α , β' , γ , and γ' phases at 1100 °C. These values are the most representative of several ones. The ferrite α and γ phases are Fe-rich and Ni-rich, respectively, as expected. Nevertheless, the β' phase is supersaturated with Fe, and its composition is far from the chemical composition of the intermetallic NiAl [55]. In contrast, the γ' phase has a chemical composition close to the intermetallic Ni_3Al [56] with a small amount of Fe. Table 2 shows the crystal structure and space group of the present phases according to the literature [57–64].

Table 1. TC-calculated chemical composition of the equilibrium phases at 1100 °C.

Phase	at.% Fe	at.% Ni	at.% Al
α	90.0	2.5	7.5
β'	45.5	13.5	41.0
γ	23.4	70.0	6.6
γ'	4.0	72.0	24.0

Table 2. Space group and crystal structure of involved phases “data from [57–64]”.

Phase	Crystal Structure (Space Group)	Elements
α	A2 (229) [57,58]	Fe [61]
β'	B2 (221) [57,59,60]	NiAl [60,61]
γ	A1 (225) [57,61,62]	Ni [62]
γ'	L1 ₂ (221) [57,62–64]	Ni ₃ Al [62]

The SEM micrographs of representative zones, as indicated by F3 in Figure 1, are shown in Figure 3a,b for the Fe/FeNiAl alloy diffusion couple side. Figure 3a shows the presence of an irregular shape of Fe γ dispersed in the β' phase, while Figure 3b shows the spheroid β' phase in the Fe α phase. These results are consistent with the ternary diagrams

in Figure 2b. In contrast, the SEM micrographs for representative zones, as indicated by F4 in Figure 1, are shown in Figure 4a,b for the Ni/FeNiAl alloy diffusion couple side. Both micrographs present the irregular shape of the γ phase dispersed in the β' phase, which also agrees with the ternary-phase diagram at 1100 °C in Figure 2b. The γ' phase is an intermetallic compound with a Ni_3Al crystalline structure. This phase commonly appears during the precipitation of Ni-based superalloy. The γ' phase also provides the creep strength for operation at high temperatures [1,65,66]. The interface between the γ' precipitate and the γ matrix phase is coherent, which is related to their excellent creep strength and coarsening resistance at high temperatures.

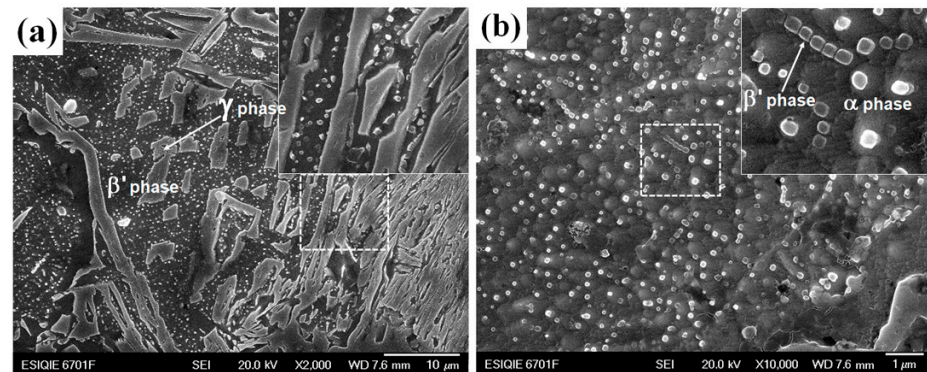


Figure 3. SEM micrographs of the Fe/Fe-Ni-Al alloy diffusion couple side, (a) irregular shapes of the γ phase dispersed in the β' phase, and (b) spheroid β' phase dispersed in the Fe α phase.

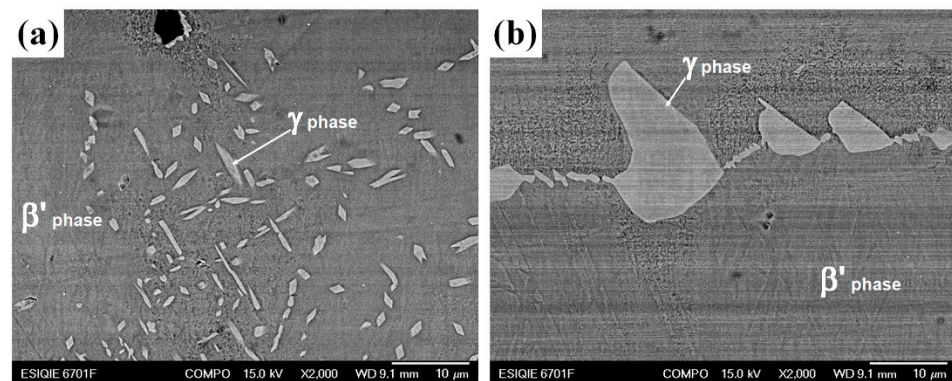


Figure 4. SEM micrographs of the Ni/Fe-Ni-Al alloy diffusion couple side, (a,b) irregular shapes of the γ phase dispersed in the β' phase.

3.2. Microstructure Evolution of Aged Diffusion Couples

The microstructure evolution of the Ni/FeNiAl alloy diffusion couple after aging at 750 °C for 100 and 250 h is shown in Figure 5a–d. These figures correspond to a region, as indicated by F5 in Figure 1. These figures indicate an evident coarsening of the γ phase in the β' phase. On the other hand, SEM micrographs of Figure 5a,b correspond to the Ni/Fe-Ni-Al alloy side aged at 750 °C for 100 and 250 h, respectively. Two precipitation reactions are present during aging at 750 °C. In the case of the γ phase, the aging treatment causes the following precipitation:



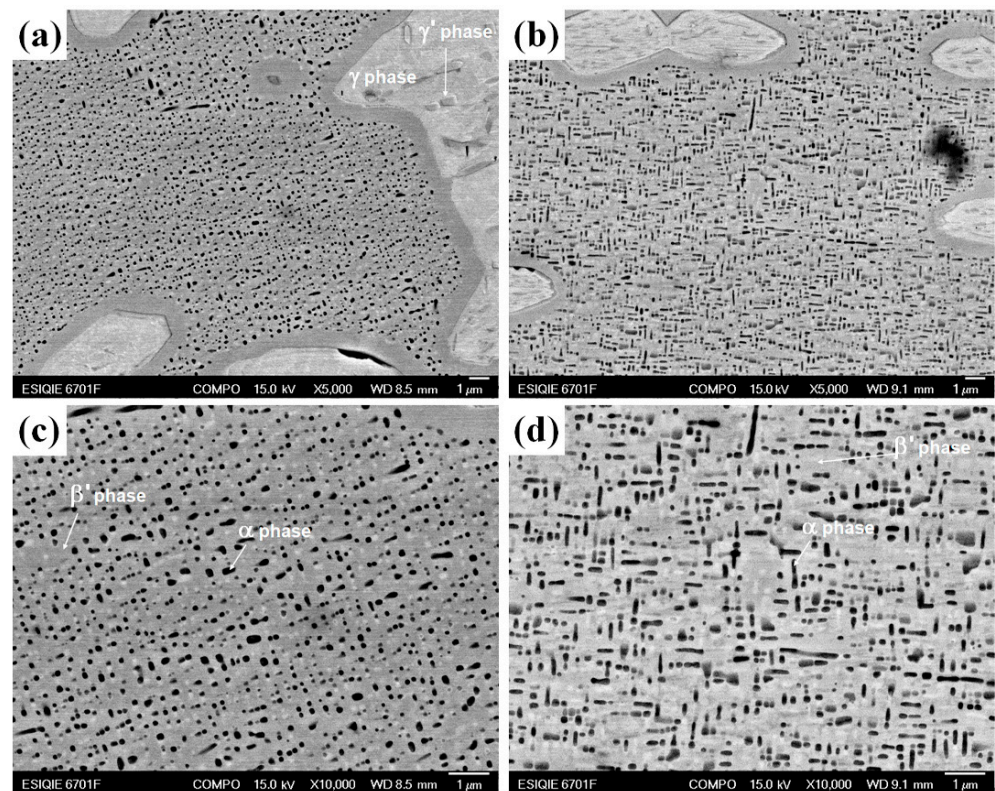


Figure 5. SEM micrographs of the Ni/Fe-Ni-Al alloy diffusion couple side after aging at 750 °C (a,c) for 100 h and (b,d) 250 h.

γ' is the Ni_3Al -type intermetallic compound. The morphology of the γ' phase is like cuboids or plates having a preferential alignment in the γ matrix, as expected for this precipitation [26]. The $\gamma + \gamma'$ zone is also present in the Fe-Ni-al phase diagram at 750 °C in Figure 2a. The γ' precipitates coarsen with time (Figure 5a,b).

In contrast, the precipitation reaction for β' phase is as follows:



That is, the soft α phase precipitates in the hard β' phase, which is considered an inverse precipitation reaction. The precipitate shape of the ferrite phase is spheroids, as shown in Figure 5c,d. This inverse precipitation is favored by increasing Ni and Al contents in the Fe-Ni-Al alloys. These precipitates also coarsen with aging time and show a preferential alignment in the β' matrix. It is important to mention that this inverse precipitation is not as common as the inverse precipitation $\gamma' \rightarrow \gamma' + \gamma$ reported [65,66] in Ni-base superalloys. This precipitation is also promoted with higher contents of Ni and Al.

The normal precipitation reaction in Fe-Ni-Al alloys [20,21] is:



This fact means the hard β' phase with a NiAl crystalline structure is formed in the bcc ferrite α phase matrix. Figure 6 illustrates the SEM micrograph of the precipitation process of the β' precipitates in the ferritic α matrix phase for a zone, as indicated by F6 in Figure 1, for the Fe/FeNiAl alloy diffusion couple after aging at 750 °C for 50 h. The $\alpha + \beta'$ region is also noted in Figure 2a.

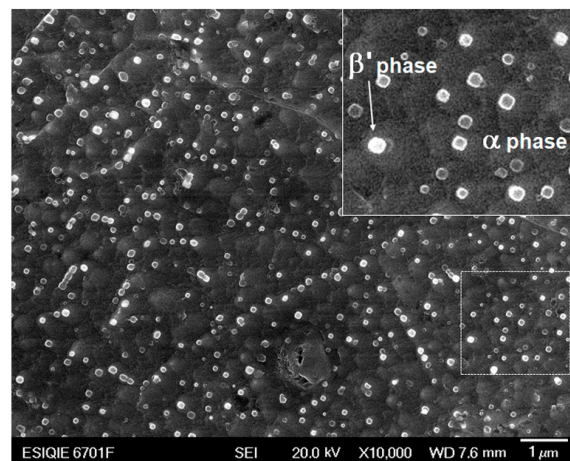


Figure 6. SEM micrographs of the Fe/Fe-Ni-Al alloy diffusion couple side after aging at 750 °C for 50 h.

Table 3 shows the TC-calculated chemical composition of the equilibrium α , β' , γ , and γ' phases at 750 °C. These compositions are representative of the chosen values. The α and γ phases become richer in Fe and in Ni, respectively, compared to the contents at 1100 °C. The Ni and Al contents of the β' phase increase, while those of the γ' phase decrease concerning the contents at 1100 °C. This behavior suggests that the solute supersaturation of the α and γ phases decreases with temperature. These solutes enrich the γ' and β' phases; however, their compositions are farther than the Ni_3Al and NiAl intermetallic compounds, respectively.

Table 3. TC-calculated chemical composition of the equilibrium phases at 750 °C.

Phase	at.% Fe	at.% Ni	at.% Al
α	93.0	2.0	5.0
β'	36.0	16.0	48.0
γ	15.0	80.0	5.0
γ'	19.0	66.0	15.0

3.3. Effect of Microstructure on Hardness

The hardness profile of the diffusion couples is shown in Figure 7a–c for the diffusion-annealed and subsequently aged at 750 °C for 100 h and 250 h, respectively. The highest average value of about 430 VHN corresponds to the region of Fe-33at.%Ni-33at.%Al alloy with the presence of the β' phase in Figure 7a. This value is attributable to the intermetallic NiAl. Nevertheless, the β' phase corresponds to a (FeNi)Al intermetallic compound [20]. The increase in Ni or Fe in the Fe-33at.%Ni-33at.%Al alloy causes a decrease in hardness, according to Figure 7a. The slight reduction in hardness of the Fe-rich side for the Fe/FeNiAl alloy diffusion couple is attributable to the presence of fine precipitates of β' in the α ferrite matrix, Figure 3b. This precipitation type could cause hardness values between 365 and 450 VHN [20,21]. In the case of the Ni-rich side of the Ni/FeNiAl alloy diffusion couple, a sudden drop in the hardness is present, which is related to the formation of a mixture of γ and β' phases (Figure 4a,b).

The reduction in hardness in the FeNiAl alloy, observed in Figure 7a,b after aging at 750 °C for 100 and 250 h, can be explained by the inverse precipitation of the α ferrite in the β' phase matrix.

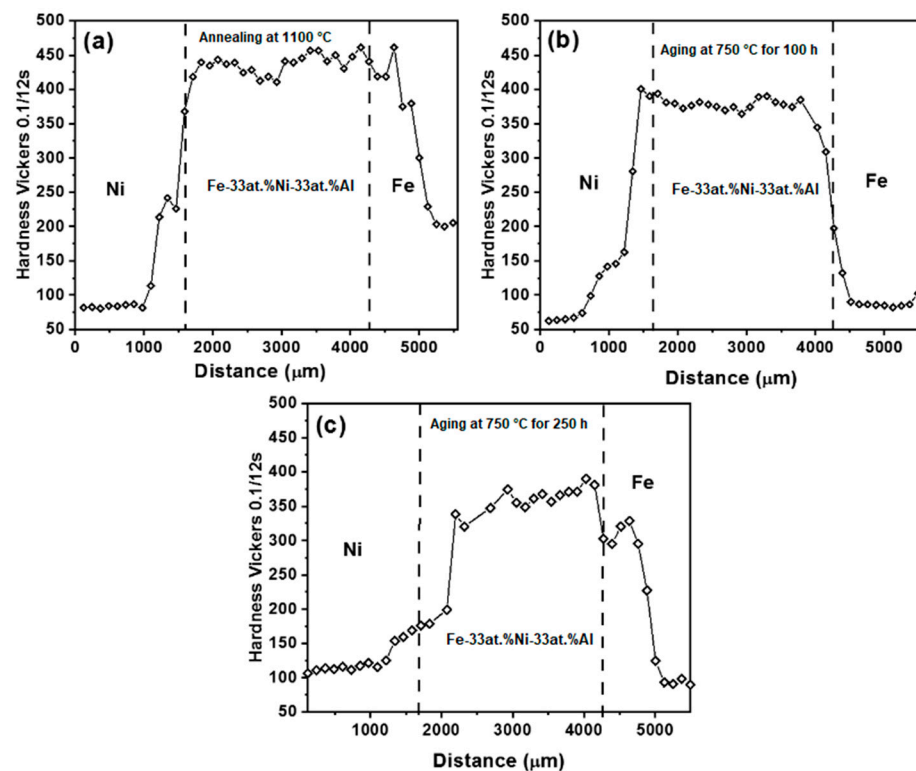


Figure 7. Vickers hardness profiles of the Fe/Fe-Ni-Al alloy/Ni diffusion couple after (a) diffusion annealing at 1100 °C, and subsequent aging at 750 °C for (b) 100 h and (c) 250 h.

3.4. Normal Precipitation versus Inverse Precipitation

Figure 8a,b present the calculated plot of volume fraction against temperature for the Fe-10at.%Ni-15at.%Al and Fe-33at.%Ni-33at.%Al alloys, respectively. The precipitation reaction, $\alpha \rightarrow \alpha + \beta'$, occurs at temperatures lower than 1050 °C in the former alloy. The precipitate amount increases with the reduction in temperature. In contrast, the inverse precipitation, $\beta' \rightarrow \beta' + \alpha$, is present for the Fe-33at.%Ni-33at.%Al alloy (Figure 8b). Moreover, the volume fraction of precipitates is higher than that of the former case. The inverse precipitation causes no precipitation hardening since the hardness of the β' phase, the (Fe,Ni)Al intermetallic compound, is higher than that of the α ferrite phase. Moreover, the volume fraction of precipitates is higher for the inverse precipitation, as shown in Figure 8b. Table 4 illustrates, for instance, the chemical composition of the matrix and precipitate for the normal precipitation and inverse precipitation alloys. In both cases, the β' phase has a chemical composition very close to that of NiAl intermetallic compounds. The chemical composition of the ferrite α phase is also very close for both alloys. This fact suggests that the difference in hardness between these alloys depends on the amount of them in the alloy. That is, the higher volume fraction of the β' phase, the higher hardness. The TC-Prisma analysis for the precipitation in these two alloy compositions is shown in Figure 9a,b for a comparison with the plot of precipitate radius as a function of time during aging at 550 °C for times up to 1000 h. This temperature was selected to cause precipitation for both alloy compositions. In the case of temperatures higher than 550 °C, the activation energy for the inverse precipitation was too high in the Fe-33at.%Ni-33at.%Al alloy, and thus no simulation results were obtained. This is attributable to the low supersaturation of the Fe solute in the β' phase [53,63]. Figure 9a corresponds to Fe-10at.%Ni-15at.%Al alloy and indicates a constant radius up to times of about 1×10^1 s. This stage is related to the nucleation process of the β' phase. Then, there is a rapid increase in radius with time up to 3×10^2 s, associated with the growth process, and the time exponent is $1/2$ for this case. In the coarsening process, there is an increase in radius with time. The growth kinetics for the coarsening stage follows the diffusion-controlled coarsening LSW theory [17,20,21,31,67]

and, thus, the exponent times are $1/3$, as expected. In contrast, in the growth kinetics behavior for the Fe-33at.%Ni-33at.%Al alloy (Figure 9b), the first two stages, nucleation and growth, are present; however, the coarsening stage is absent for the aging time of 1×10^4 s (1000 h). This difference suggests that the growth kinetics are faster for the former alloy than for the latter one. Moreover, the higher solute content also favors a slower diffusion process [52,53]. This behavior is attributable to the faster diffusion process in the α ferrite matrix for the former alloy than that of the intermetallic compound β' matrix phase. The slower kinetics for the Fe-33at.%Ni-33at.%Al alloy permits expecting higher coarsening resistance during heating. The TC-Prisma-calculated interfacial free energy for the interface β' precipitate and α matrix and the α precipitate and β' matrix were 0.173 and 0.183 Jm⁻², respectively. These energy values are very close, and they are lower than 0.2 Jm⁻². This fact suggests a coherent interface between the precipitate and matrix, which improves their mechanical strength and coarsening resistance for both alloys.

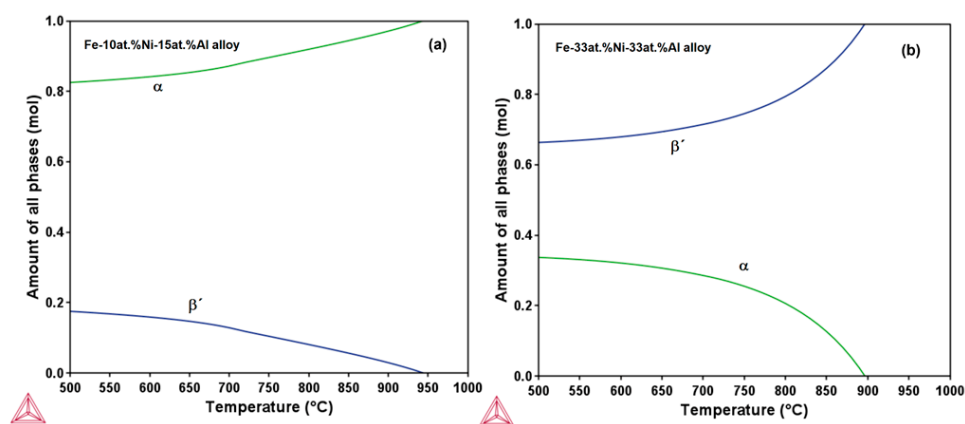


Figure 8. TC-calculated plot of amount of equilibrium phases versus temperature for the (a) Fe-10at.%Ni-15at.%Al and (b) Fe-33at.%Ni-33at.%Al alloys.

Table 4. TC-calculated chemical composition of the equilibrium α and β' phases at 550 °C.

Alloy	Phase	at.% Fe	at.% Ni	at.% Al
Fe-10at.%Ni-15at.%Al	α	89.5	1.5	9.0
	β'	9.5	48.5	42.0
Fe-33at.%Ni-33at.%Al	α	88.6	1.2	10.2
	β'	8.3	48.0	43.7

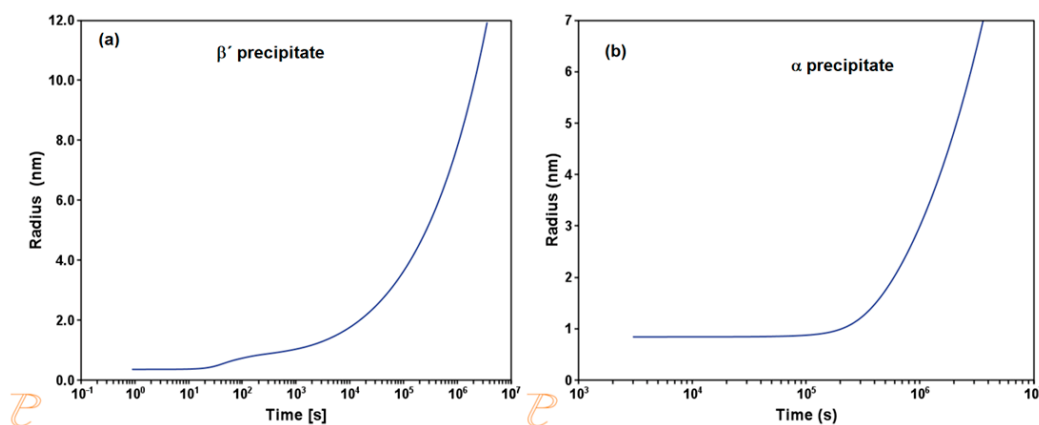


Figure 9. TC-Prisma precipitate radius versus time for the (a) Fe-10at.%Ni-15at.%Al and (b) Fe-33at.%Ni-33at.%Al alloys aged at 550 °C.

4. Conclusions

The Calphad-based numerical and diffusion couple analyses permit us to conclude the following:

- a. The Calphad-based diffusion paths for the Fe/Fe-Ni-Al alloy/Ni diffusion couples are in good agreement with the experimental ones for diffusion annealing at 1100 °C.
- b. The equilibrium phases formed during the annealing at 1100 °C are consistent with the Calphad-calculated Fe-Ni-Al phase diagram at the same temperature.
- c. The precipitation reactions of $\alpha \rightarrow \alpha + \beta'$ and $\gamma \rightarrow \gamma + \gamma'$ occurred during aging at 750 °C, promoting the precipitation hardening.
- d. The presence of the inverse precipitation reaction, $\beta' \rightarrow \beta' + \alpha$, caused a decrease in hardness because of the precipitation of the soft α ferrite phase. This fact indicates that inverse precipitation is also possible for Fe-based superalloys, as observed in Ni-based superalloys.
- e. The coarsening process of α precipitates is slower than that of the β' precipitates during the aging of the Fe-Ni-Al alloys, which suggests a better response of the latter precipitate to coarsening during service operation.

Author Contributions: Conceptualization, E.P.-B., H.J.D.-R. and V.M.L.-H.; methodology, E.P.-B. and M.L.S.-M.; software, E.P.-B. and V.M.L.-H.; validation, H.J.D.-R. and E.P.-B.; formal analysis, E.P.-B. and V.M.L.-H.; investigation, E.P.-B. and M.L.S.-M.; writing original draft preparation, E.P.-B., V.M.L.-H. and H.J.D.-R. All authors have read and agreed to the published version of the manuscript.

Funding: This research received no external funding.

Institutional Review Board Statement: Not applicable.

Informed Consent Statement: Not applicable.

Data Availability Statement: The data that support the findings of this study are available from the corresponding author upon request.

Acknowledgments: The authors acknowledge the financial support from CONACYT and SIP-BEIFI-IPN.

Conflicts of Interest: The authors declare no conflict of interest.

References

1. Chen, Y.; Prasath Babu, R.; Slater, T.J.; Bai, M.; Mitchell, R.; Ciuca, O.; Preuss, M.; Haigh, S.J. An investigation of diffusion-mediated cyclic coarsening and reversal coarsening in an advanced Ni-based superalloy. *Acta Mater.* **2016**, *110*, 295–305. [[CrossRef](#)]
2. Liu, D.Y.; Zhao, M.J.; Tao, N.R. Precipitation and its hardening behavior in an austenitic steel with different strain-induced structures. *Scr. Mater.* **2023**, *230*, 115396. [[CrossRef](#)]
3. Huang, Y.S.; Wang, X.G.; Cui, C.Y.; Li, J.G.; Ye, L.H.; Hou, G.C.; Yang, Y.H.; Liu, J.L.; Liu, J.G.; Zhou, Y.Z.; et al. The effect of coarsening of γ' precipitate on creep properties of Ni-based single crystal superalloys during long-term aging. *Mater. Sci. Eng. A* **2020**, *773*, 138886. [[CrossRef](#)]
4. Hardy, M.C.; Detrois, M.; McDevitt, E.T.; Argyrakis, C.; Saraf, V.; Jablonski, P.D.; Hawk, J.A.; Buckingham, R.C.; Kitaguchi, H.S.; Tin, S. Solving recent challenges for wrought Ni-based superalloys. *Metall. Mater. Trans. A* **2020**, *51*, 2626–2650. [[CrossRef](#)]
5. Degeiter, M.; Le Bouar, Y.; Appolaire, B.; Perrut, M.; Finel, A. Instabilities in the periodic arrangement of elastically interacting precipitates in nickel-based superalloys. *Acta Mater.* **2020**, *187*, 41–50. [[CrossRef](#)]
6. Zhang, R.Y.; Qin, H.L.; Bi, Z.N.; Li, J.; Paul, S.; Lee, T.L.; Zhang, S.Y.; Zhang, J.; Dong, H.B. Evolution of lattice spacing of gamma double prime precipitates during aging of polycrystalline Ni-based superalloys: An in situ investigation. *Metall. Mater. Trans. A* **2020**, *51*, 574–585. [[CrossRef](#)]
7. Zhang, L.; Wen, Y.; Liu, Y.; Quan, F.; Han, J.; Yang, S.; Chen, X.; He, S.; Gorbatov, O.I.; Chen, X.; et al. Cr-promoted formation of B2+L2₁ composite nanoprecipitates and enhanced mechanical properties in ferritic alloy. *Acta Mater.* **2023**, *243*, 118506. [[CrossRef](#)]
8. Sahoo, B.K.; Srivastava, V.C.; Chandan, K.A.; Chowdhury, S.G. Enhancing the properties of Al–Ni added medium Mn steel by tailoring B2–NiAl precipitates through aging treatment. *Mater. Sci. Eng. A* **2022**, *837*, 142757. [[CrossRef](#)]
9. Muñoz-Morris, M.A.; Morris, D.G. Microstructure and mechanical behavior of a Fe-Ni-Al alloy. *Mater. Sci. Eng. A* **2007**, *444*, 236–241. [[CrossRef](#)]
10. Stallybrass, C.; Schneide, A.; Sauthoff, G. The strengthening effect of (Ni,Fe)Al precipitates on the mechanical properties at high temperatures of ferritic Fe–Al–Ni–Cr alloys. *Intermetallics* **2005**, *13*, 1263–1268. [[CrossRef](#)]
11. Stallybrass, C.; Sauthoff, G. Ferritic Fe–Al–Ni–Cr alloys with coherent precipitates for high-temperature applications. *Mater. Sci. Eng. A* **2004**, *387*, 985–990. [[CrossRef](#)]

12. Vo, N.Q.; Liebscher, C.H.; Rawlings, M.J.S.; Asta, M.; Dunand, D.C. Creep properties and microstructure of a precipitation-strengthened ferritic Fe-Al-Ni-Cr alloy. *Acta Mater.* **2014**, *71*, 89–99. [[CrossRef](#)]
13. Teng, Z.K.; Liu, C.T.; Ghosh, G.; Liaw, P.K.; Fine, M.E. Effects of Al on the microstructure and ductility of NiAl-strengthened ferritic steels at room temperature. *Intermetallics* **2010**, *18*, 1437–1443. [[CrossRef](#)]
14. Sun, L.; Simm, T.H.; Martin, T.L.; McAdam, S.; Galvin, D.R.; Perkins, K.M.; Bagot, P.A.J.; Moody, M.P.; Ooi, S.W.; Hill, P.; et al. A novel ultra-high strength maraging steel with balanced ductility and creep resistance achieved by nanoscale β -NiAl and Laves phase precipitates. *Acta Mater.* **2018**, *149*, 285–301. [[CrossRef](#)]
15. Yong, L.; Zou, Y.; Peng, H.; Chen, J.; Fan, Q.; Yang, Q.; Yan, J.; Huang, S.; Wen, Y. Precipitation behavior of coherent nano-ordered particles in Fe-Mn-Al-Ni shape memory alloys with different Ni contents. *Mater. Charact.* **2022**, *188*, 111912. [[CrossRef](#)]
16. Ann, Y.F.; Chen, X.P.; Mei, L.; Ren, P.; Wei, D.; Cao, W.Q. Precipitation transformation pathway and mechanical behavior of nanoprecipitation strengthened Fe-Mn-Al-C-Ni austenitic low-density steel. *J. Mater. Sci.* **2023**, *in press*.
17. Baik, S.I.; Rawlings, M.J.S.; Dunand, D.C. Effect of aging on coarsening and creep resistance of a Ti-modified Fe-Ni-Al-Cr-Mo ferritic steel with L₂₁/B2 composite precipitates. *Mater. Sci. Eng. A* **2020**, *776*, 138987. [[CrossRef](#)]
18. Song, G.; Hong, S.J.; Song, S.H.; Hong, S.H.; Kim, K.B.; Liaw, P.K. Optimization of B2/L₂₁ hierarchical precipitate structure to improve creep resistance of a ferritic Fe-Ni-Al-Cr-Ti superalloy via thermal treatments. *Scr. Mater.* **2019**, *161*, 18–22. [[CrossRef](#)]
19. Basuki, E.A.; Nababan, D.C.; Muhammad, F.; Korda, A.A.; Prajitno, D.H. Isotherm mal Oxidation Behaviour of 69.5Fe-14Ni-9Al-7.5Cr Alloy at High Temperatures. *Int. J. Corros.* **2019**, *2019*, 8517648. [[CrossRef](#)]
20. Rosales-Dorantes, H.J.; Cayetano-Castro, N.; Lopez-Hirata, V.M.; Saucedo-Muñoz, M.L.; Villegas-Cardenas, J.D.; Hernández-Santiago, F. Coarsening process of coherent β' precipitates in Fe-10 wt-%Ni-15 wt-%Al and Fe-10 wt-%Ni-15 wt-%Al-1 wt-%Cu alloys. *Mater. Sci. Technol.* **2013**, *29*, 1492–1498. [[CrossRef](#)]
21. Ferreira-Palma, C.; Contreras-Piedras, E.; Cayetano-Castro, N.; Saucedo-Muñoz, M.L.; Lopez-Hirata, V.M.; Gonzalez-Velazquez, J.L.; Dorantes-Rosales, H.J. Effect of temperature and composition on NiAl precipitation and morphology in Fe-Ni-Al alloys. *Metall. Mater. Trans. A* **2017**, *48*, 5285–5293. [[CrossRef](#)]
22. Dorantes-Rosales, H.J.; Cayetano-Castro, N.; Cruz-Rivera, J.J.; López-Hirata, V.M.; González-Velázquez, J.L.; Moreno-Palmerín, J. Cinética de engrosamiento de precipitados coherentes en aleaciones base hierro. *Rev. Latinoam. Metal. Mater.* **2009**, *2*, 637–645.
23. Zhou, X.; Dong, H.; Wang, Y.; Yuan, M. Microstructure characteristics and mechanical performance of Fe-Cr-Ni-Al-Ti superalloy fabricated by powder metallurgy. *J. Alloys Compd.* **2022**, *918*, 165612. [[CrossRef](#)]
24. Xing, Z.; Pang, J.; Zhang, H.; Ji, Y.; Zhu, Z.; Wang, A.; Zhang, L.; Li, H.; Fu, H.; Zhang, H. Optimizing the microstructure and mechanical performance of Fe-Ni-Cr-Al high entropy alloys via Ti addition. *J. Alloys Compd.* **2020**, *943*, 169149. [[CrossRef](#)]
25. Song, G.; Sun, Z.; Poplawsky, J.D.; Gao, Y.; Liaw, P.K. Microstructure evolution of single Ni₂TiAl or hierarchical NiAl/Ni₂TiAl precipitates in Fe-Ni-Al-Cr-Ti ferritic alloys during thermal treatment for elevated-temperature applications. *Acta Mater.* **2017**, *127*, 1–16. [[CrossRef](#)]
26. Baldan, A. Progress in Ostwald ripening theories and their applications to nickel-base superalloys. *J. Mater. Sci.* **2002**, *37*, 2171–2202. [[CrossRef](#)]
27. Shen, Q.; Xiong, X.; Li, T.; Cheng, Y.; Liu, W. Effect of co-addition of Ni and Al on precipitation evolution and mechanical properties of Fe-Cu alloy. *Mater. Sci. Eng. A* **2018**, *723*, 279–286. [[CrossRef](#)]
28. Baik, S.I.; Rawlings, M.J.S.; Dunand, D.C. Effect of hafnium micro-addition on precipitate microstructure and creep properties of a Fe-Ni-Al-Cr-Ti ferritic superalloy. *Acta Mater.* **2018**, *153*, 126–135. [[CrossRef](#)]
29. Rawlings, M.J.S.; Dunand, D.C. Dislocation dynamics modeling of precipitation strengthening in Fe-Ni-Al-Cr ferritic superalloys. *J. Mater. Res.* **2017**, *32*, 4241–4253. [[CrossRef](#)]
30. Zeisl, S.; Landefeld, A.; Van Steenberge, N.; Chang, Y.; Schnitzer, R. The role of alloying elements in NiAl and Ni₃Ti strengthened Co-free maraging steels. *Mater. Sci. Eng. A* **2022**, *861*, 144313. [[CrossRef](#)]
31. Contreras-Piedras, E.; Dorantes-Rosales, H.J.; Lopez-Hirata, V.M.; Hernandez-Santiago, F.; Gonzalez-Velazquez, J.L.; Lopez-Monroy, F.I. Analysis of precipitation in Fe-rich Fe-Ni-Al alloys by diffusion couples. *Mater. Sci. Eng. A* **2012**, *558*, 366–370. [[CrossRef](#)]
32. Dong, K.; Sun, L.; Zhang, Z.; Li, Z.; Li, J.; Liu, L.; Du, K.; Zhang, Y. Effects of V addition on microstructure and pseudoelastic response in Fe-Mn-Al-Ni alloys. *Intermetallics* **2023**, *160*, 107954. [[CrossRef](#)]
33. Park, K.; Cho, B.; Hong, S.J.; Lim, K.R.; Lee, C.; Song, G. Outstanding high-temperature strength of novel Fe-Cr-Ni-Al-V ferritic alloys with hierarchical B2-NiAl precipitates. *Mater. Sci. Eng. A* **2022**, *840*, 142999. [[CrossRef](#)]
34. Eris, R.; Akdeniz, M.V.; Mekhrabov, A.O. Unveiling the effect of Hf-(Mo,W) addition on the coarsening agglomeration, and dissolution behaviour of γ' -Ni₃Al precipitates in model Ni-based superalloys. *J. Alloys Compd.* **2023**, *936*, 167869. [[CrossRef](#)]
35. Baik, S.I.; Wang, S.Y.; Liaw, P.K.; Dunand, D.C. Increasing the creep resistance of Fe-Ni-Al-Cr superalloys via Ti additions by optimizing the B2/L₂₁ ratio in composite nano-precipitates. *Acta Mater.* **2018**, *157*, 142–154. [[CrossRef](#)]
36. Sohn, Y.H.; Puccio, A.; Dayananda, M.A. Interdiffusion structures and paths for multiphase Fe-Ni-Al diffusion couples at 1100 °C. *Metall. Mater. Trans. A* **2005**, *36*, 2361–2370. [[CrossRef](#)]
37. Miyazaki, T.; Koyama, T.; Kobayashi, S. A new characterization method of the microstructure using microscopic gradients in alloys. *Metall. Mater. Trans. A* **1996**, *27*, 945–949. [[CrossRef](#)]
38. Cao, S.; Zhao, J.-C. Application of dual-anneal diffusion multiples to the effective study of phase diagrams and phase transformations in the Fe-Cr-Ni system. *Acta Mater.* **2015**, *88*, 196–206. [[CrossRef](#)]

39. Shi, P.; Engstrom, A.; Hoglund, L.; Sundman, B.; Agren, J. Thermo-calc and DICTRA enhance materials design and processing. *Mater. Sci. For.* **2005**, *475–479*, 3339–3346.
40. Borgestam, A.; Hoglund, L.; Agren, J.; Engstrorn, A. DICTRA, a tool for simulation of diffusional transformations in alloys. *J. Phase Equil.* **2000**, *21*, 269–280. [[CrossRef](#)]
41. Wu, Q.; Xu, G.; Chang, H.; Zhou, L.; Cui, Y. Assessment of diffusion mobility for bcc phase of Ti-Al-Ni ternary system. *Calphad* **2020**, *71*, 102203. [[CrossRef](#)]
42. Dictra, Thermo-Calc Software Versión 2023a. Available online: <https://thermocalc.com/products/add-on-modules/diffusion-module-dictra/> (accessed on 1 June 2023).
43. Thermo-Calc, Thermo-Calc Software version 2023a, TCFE11 and MOBFE6 Steel/Fe Alloys Databases. Available online: <https://thermocalc.com/products/databases/steel-and-fe-alloys/> (accessed on 1 June 2023).
44. Sundman, B.; Ohnuma, I.; Dupin, N.; Kattner, U.R.; Fries, S.G. An assessment of the entire Al-Fe system including D0₃ ordering. *Acta Mater.* **2009**, *57*, 2896–2908. [[CrossRef](#)]
45. Lindahl, B.B.; Burton, B.P.; Selleby, M. Ordering in ternary BCC alloys applied to the Al-Fe-Mn system. *Calphad* **2015**, *51*, 211–219. [[CrossRef](#)]
46. Hu, X.X.; Lu, X.G.; He, Y.L. Assessments of impurity diffusion coefficients of selected pure metals in FCC Fe. *Adv. Mater. Res.* **2014**, *936*, 545–551. [[CrossRef](#)]
47. Bokstein, B.S.; Bokstein, S.Z.; Spitsberg, I.T. Ni self-diffusion in alloyed Ni₃Al. *Intermetallics* **1996**, *4*, 517–523. [[CrossRef](#)]
48. Zhang, L.; Du, Y.; Steinbach, I.; Chen, Q.; Huang, B. Diffusivities of an Al-Fe-Ni melt and their effects on the microstructure during solidification. *Acta Mater.* **2010**, *10*, 3664–3675. [[CrossRef](#)]
49. Engström, A.; Agren, J. Interdiffusion in multiphase, Fe-Cr-Ni diffusion couples. *Scand. J. Metall.* **1995**, *24*, 12–20.
50. Hood, G.M. The diffusion of iron in aluminium. *J. Theor. Appl. Phys.* **1970**, *21*, 305–328. [[CrossRef](#)]
51. Gao, X.; Wang, H.; Ma, C.; Lv, M.; Ren, H. Segregation of alloying elements at the bcc-Fe/B2-NiAl interface and the corresponding effects on the interfacial energy. *Intermetallics* **2021**, *131*, 107096. [[CrossRef](#)]
52. Mehrer, H. Diffusion in Solid Metals and Alloys. In *Landolt-Börnstein—Group III Condensed Matter*; Springer: Berlin/Heidelberg, Germany, 1990; Volume 26, pp. 288–312.
53. Porter, D.A.; Easterling, K.E.; Sherif, M.Y. *Phase Transformations in Metals and Alloys*, 4th ed.; CRC Press: Boca Raton, FL, USA, 2022; pp. 96–98.
54. Kostorz, K. *Phase Transformations in Materials*, 2nd ed.; Wiley-VCH: Weinheim, Germany, 2001; pp. 309–407.
55. Pavarova, K.B.; Filin, S.A.; Maslenkov, S.B. Phase equilibria in the Ni-Al-Me (Me = Co, Fe, Mn, Cu) system in vicinity of β -phase at 900 and 1100 °C. *Russ. Metall. (Engl. Transl.)* **1993**, *1*, 156–169.
56. Bramfitt, B.L.; Michael, J.R. Microanalysis of phase equilibria in Ni₃Al intermetallic alloys containing iron. *MRS Online Proc. Libr.* **1985**, *62*, 201–208. [[CrossRef](#)]
57. Looijenga-Vos, A.; Buerger, M.J. *International Tables of Crystallography Space-Group Symmetry*, 5th ed.; Hahn, T., Ed.; Springer: Dordrecht, The Netherlands, 2005; Volume A, pp. 52–53.
58. Dubrovinskaia, N.A.; Dubrovinsky, L.S.; Karlsson, A.; Saxena, S.K. Experimental study of thermal expansion and phase transformations in iron-rich Fe-Al alloys. *Calphad* **1999**, *23*, 69–84. [[CrossRef](#)]
59. Bitterlich, H.; Löser, W.; Schultz, L. Reassessment of Ni-Al and Ni-Fe-Al solidus temperatures. *J. Phase Equilibria Diffus.* **2002**, *23*, 301–304. [[CrossRef](#)]
60. Tan, Y.; Shinoda, T.; Mishima, Y.; Suzuki, T. Stoichiometry splitting of β phase in Ni-Al-Mn, Ni-Al-Co and Ni-Al-Fe ternary systems. *Mater. Trans.* **2001**, *42*, 464–470. [[CrossRef](#)]
61. Budberg, P.; Prince, A.; Cacciamani, G.; Ferro, R.; Grushko, B.; Perrot, P.; Schmid-Fetzer, R. Al-Fe-Ni (Aluminium–Iron–Nickel) Light Metal Systems Part 2. In *Landolt-Börnstein—Group IV Physical Chemistry*; Springer: Berlin/Heidelberg, Germany, 2005; Volume 11A2, pp. 345–346.
62. Belan, J. GCP and TCP phases presented in nickel-base superalloys. *Mater. Today* **2016**, *3*, 936–941. [[CrossRef](#)]
63. Alabbad, B.; Li, L.; Tin, S. Controlling the grain boundary morphology and secondary γ' precipitate size distribution in Ni-based superalloys. *J. Alloys Compd.* **2019**, *775*, 931–941. [[CrossRef](#)]
64. Turichin, G.A.; Klimova-Korsmik, O.G.; Valdaytseva, E.A.; Alekseev, A.V.; Rashkovets, M.V. Comparative analysis of the gamma prime phase formation in nickel alloys in additive manufacturing. *Procedia CIRP* **2020**, *94*, 320–323. [[CrossRef](#)]
65. Vogel, F.; Ngai, S.; Fricke, K.; McKechnie, M.; Wanderka, N.; Hentrich, T.; Banhart, J.; Thompson, G.B. Tracing the three-dimensional nanochemistry of phase separation in an inverse Ni-based superalloy. *Acta Mater.* **2018**, *157*, 326–338. [[CrossRef](#)]
66. Vogel, F.; Wanderka, N.; Balogh, Z.; Ibrahim, M.; Stender, P.; Schmitz, G.; Fedorova, T.; Banhart, J. Evolution of nanoscale clusters in γ' precipitates of a Ni-Al-Ti model alloy. *Ultramicroscopy* **2015**, *159*, 278–284. [[CrossRef](#)]
67. Kumar, A.S.D.; Bhaskar, M.S.; Sarkar, S.; Abinandanan, T.A. Phase field modelling of precipitation coarsening in binary alloys with respect to atomic mobility of solute in the precipitate phase. *Trans. Indian Inst. Met.* **2020**, *73*, 1469–1474. [[CrossRef](#)]

Disclaimer/Publisher’s Note: The statements, opinions and data contained in all publications are solely those of the individual author(s) and contributor(s) and not of MDPI and/or the editor(s). MDPI and/or the editor(s) disclaim responsibility for any injury to people or property resulting from any ideas, methods, instructions or products referred to in the content.